

# Random survival forests with multivariate longitudinal endogenous covariates

Statistical Methods in Medical Research

2023, Vol. 32(12) 2331–2346

© The Author(s) 2023

Article reuse guidelines:

sagepub.com/journals-permissions

DOI: 10.1177/09622802231206477

journals.sagepub.com/home/smm



Anthony Devaux<sup>1,2,3</sup> , Catherine Helmer<sup>1</sup>,  
Robin Genuer<sup>4,\*</sup> and Cécile Proust-Lima<sup>1,\*</sup>

## Abstract

Predicting the individual risk of clinical events using the complete patient history is a major challenge in personalized medicine. Analytical methods have to account for a possibly large number of time-dependent predictors, which are often characterized by irregular and error-prone measurements, and are truncated early by the event. In this work, we extended the competing-risk random survival forests to handle such endogenous longitudinal predictors when predicting event probabilities. The method, implemented in the R package *DynForest*, internally transforms the time-dependent predictors at each node of each tree into time-fixed features (using mixed models) that can then be used as splitting candidates. The final individual event probability is computed as the average of leaf-specific Aalen–Johansen estimators over the trees. Using simulations, we compared the performances of *DynForest* to accurately predict an event with (i) a joint modeling alternative when considering two longitudinal predictors only, and with (ii) a regression calibration method that ignores the informative truncation by the event when dealing with a large number of longitudinal predictors. Through an application in dementia research, we also illustrated how *DynForest* can be used to develop a dynamic prediction tool for dementia from multimodal repeated markers, and quantify the importance of each marker.

## Keywords

Individual dynamic prediction, multivariate predictors, random survival forest, longitudinal data, survival data, competing risks

## 1 Introduction

Quantifying the patient specific risk of disease or health events related to a disease progression based on patient's information has become a crucial issue in modern medicine. This may be done in order to monitor the disease progression, and adapt therapeutic strategies and medical choices according to their risk. One strategy is to predict the risk of event using only the data collected at the prediction time. However, in many contexts, patients data include repeated measures of markers which trajectories are highly predictive of the event. This is the case for instance with prostate specific antigen for the risk of prostate cancer recurrence<sup>1</sup> or serum creatinine for the risk of kidney graft failure.<sup>2</sup> In other contexts, such as in cardiovascular disease, not only one specific marker but many potential markers may be relevant.<sup>3</sup>

Longitudinal markers are endogenous variables in the sense that they may be affected by the event of interest,<sup>4</sup> and are usually measured intermittently with a measurement error. This makes their statistical analysis challenging.

<sup>1</sup>Univ. Bordeaux, INSERM, BPH, U1219, Bordeaux, France

<sup>2</sup>The George Institute for Global Health, UNSW Sydney, Australia

<sup>3</sup>School of Population Health, UNSW Sydney, Australia

<sup>4</sup>Univ. Bordeaux, INSERM, INRIA, BPH, U1219, Bordeaux, France

\*These authors contributed equally to this work.

## Corresponding author:

Robin Genuer, Univ. Bordeaux, INSERM, INRIA, BPH, U1219, F-33000 Bordeaux, France.

Email: robin.genuer@u-bordeaux.fr

Three approaches were proposed in the literature for the prediction of a clinical event given longitudinal endogenous information: *landmark approach*,<sup>5</sup> *joint models*,<sup>1</sup> and *regression calibration* techniques.<sup>6</sup>

Landmark approach consists in considering only the subjects still at risk of the event at a prediction time  $t$  (called landmark time) and including their information collected until  $t$  to build a prediction tool for subsequent risk of event.<sup>5,7</sup> The longitudinal information of intermittently measured and prone-to-error markers up to  $t$  can be included after a pre-processing step, by mixed models for instance.<sup>1,3,8,9</sup> In multivariate settings, the Cox model may be replaced by more advanced techniques coming from statistical learning and adapted to survival data<sup>8,9</sup> to account for the possibly large dimension of the predictors and their correlation. The landmark approach is relatively easy to implement and was shown to be robust to the misspecification of the marker trajectory or to the proportional assumption in the Cox model.<sup>7</sup> This makes it an appealing approach for extending the concept of individual dynamic prediction from a unique longitudinal marker to predictions from multivariate longitudinal markers. However, because it only relies on subjects at risk at the landmark time and exploits only the longitudinal information up to the landmark time, it suffers from a lack of efficiency, and is restricted to pre-determined prediction times.

When longitudinal and survival processes are inter-related as assumed in the dynamic prediction context, the joint modeling framework constitutes the most appropriate approach to handle this mutual dependence.<sup>4</sup> Joint models (JMs) simultaneously model the longitudinal and survival processes over time while accounting for their association using shared latent quantities; and the posterior conditional individual probability of event given the longitudinal predictor history can be easily deduced. Initially developed for a single longitudinal predictor,<sup>1</sup> the method was then extended to a few longitudinal predictors.<sup>10,11</sup> In contrast with landmark approaches, JM exploit all the available longitudinal information to build the prediction tool, thus leading to a better efficiency. However, their performances are very sensitive to the correct specification of the model.<sup>7</sup> Moreover, due to the complexity of their estimation, they are currently limited to a small number of longitudinal markers (usually 2 or 3) and thus cannot be used to predict individual risk of event in more complex settings.<sup>12</sup>

In the context of a large to high number of longitudinal predictors, regression calibration (RC) techniques were proposed as an alternative to JM. RC is a two-stage approach which first summarizes the longitudinal predictors into time-fixed features as in the landmark approach but using all the repeated measures until the time of event or censoring, and then includes the features into prediction models. Several RC methods have been proposed with a first step using mixed models or functional data analysis<sup>13</sup> to summarize the multiple longitudinal predictors. Then, the Cox model,<sup>14</sup> penalized regression<sup>15</sup> or random survival forests<sup>16,17</sup> have been used to derive the risk prediction. As in JM, RC techniques include all the available information on the markers and survival during the follow-up to build the prediction tool. However, they neglect the informative truncation of the longitudinal data due to the event, which can bias the estimates and impact the prediction accuracy.<sup>18</sup>

In this work, we propose a novel methodology based on the competing-risk random survival forests (RSFs)<sup>19,20</sup> to accurately predict a risk of event from possibly large-dimensional longitudinal predictors. RSFs have become popular for prediction tasks as they can handle a high number of covariates and capture potentially complex associations. However, RSFs have been limited so far to time-independent predictors. To extend RSF to intermittently measured and error-prone longitudinal predictors, we model them using linear mixed models. However, in contrast to the landmark and RC techniques, we directly incorporate those computations at each recursive step of the RSF tree building to better handle the informative truncation of the longitudinal endogenous data and thus provide more appropriate and accurate individual predictions. Furthermore, to better understand which variables are the most useful in obtaining the predictions and ease the interpretation of the results, we generalized the permutation-based variable importance index of RSF to longitudinal markers.

The rest of this article is organized as follows. Section 2 introduces our extended random survival forest methodology, called DynForest, and describes how it can handle time-dependent endogenous predictors to predict a risk of event, possibly with multiple causes. Section 3 describes an extensive simulation study which aimed at validating DynForest methodology and at contrasting its performances with those of alternative approaches. In Section 4, DynForest is applied in a large population-based French cohort to predict the probability of experiencing a dementia before death from multiple markers stemming from neuropsychological evaluation, clinical evaluation and brain magnetic resonance imaging (MRI), and identify the importance of each type of markers. Finally, Section 5 closes the work with a discussion.

## 2 Methods

### 2.1 Framework and notations

We consider a sample of  $N$  subjects. For each individual  $i \in \{1, \dots, N\}$ , we denote  $T_i$  the event time,  $C_i$  the independent censoring time, and  $\tilde{T}_i = \min(T_i, C_i)$  the observed time of event. We define  $\delta_i$  the indicator of the cause of event with  $\delta_i = k$

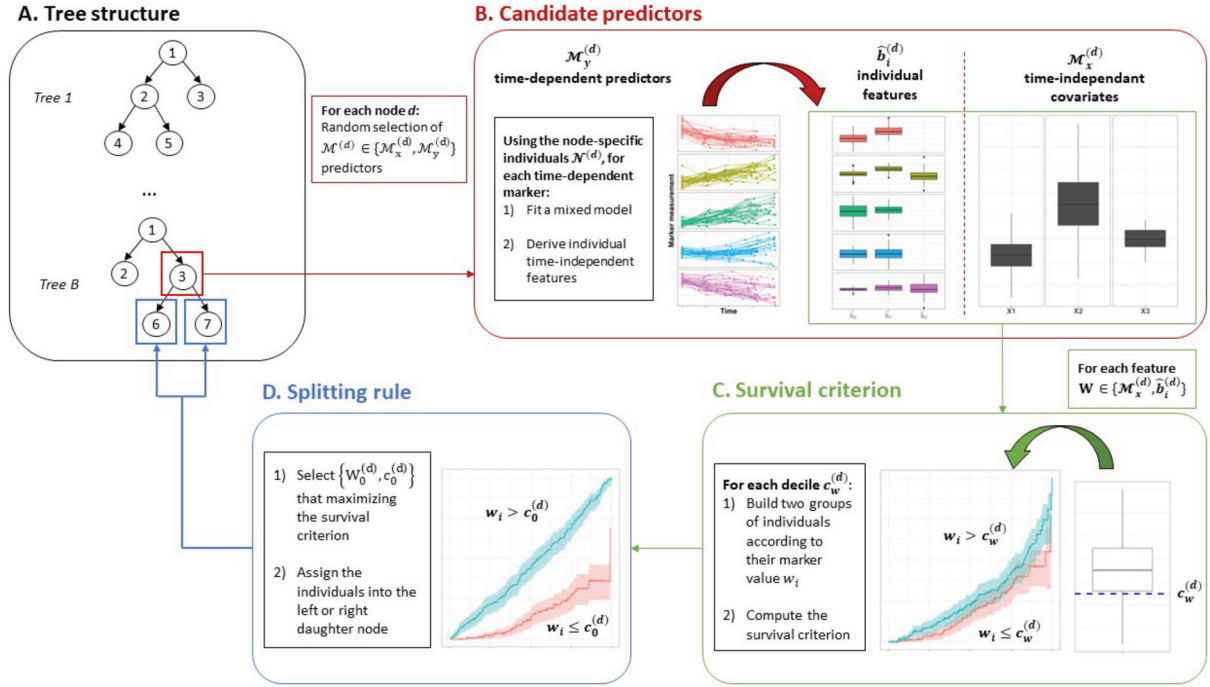


**Figure 1.** Overall scheme of the tree building in DynForest with (A) the tree structure, (B) the node-specific treatment of time-dependent predictors to obtain time-fixed features, (C) the dichotomization of the time-fixed features, and (D) the splitting rule.

if subject experiences the event of cause  $k \in \{1, \dots, K\}$  before censoring and  $\delta_i = 0$  otherwise. We observe an ensemble  $\mathcal{M}_x$  of  $P$  time-independent covariates  $X_{ip}$  ( $p = 1, \dots, P$ ), and an ensemble  $\mathcal{M}_y$  of  $Q$  time-dependent covariates  $Y_{ijm}$ , for  $m = 1, \dots, Q$  measured at subject-and-covariate-specific times  $t_{ijm}$ , with  $j = 1, \dots, n_{im}$  the occasion and  $t_{ijm} \leq \tilde{T}_i$ .

Our methodology consists of a RSF that incorporates an internal processing for handling time-dependent covariates. A RSF is an ensemble of  $B$  survival decision trees that are ultimately aggregated together. Each tree  $b \in \{1, \dots, B\}$  is built from a bootstrap sample of the original sample of  $N$  subjects. This results, on average, in the exclusion of 37% of the subjects that constitute the out-of-bag (OOB) sample, noted  $OOB^b$ .

## 2.2 The tree building

A tree is a recursive procedure designed to partition the subjects into homogeneous groups regarding the outcome of interest. The overall tree building procedure is summarized in Figure 1. Each tree recursively splits the bootstrap sample into two subgroups at junctions called nodes until the subgroups reach a minimal size. At each node  $d \in \mathcal{D}$ , the split is determined according to a dichotomized feature that maximizes the distance between the two groups; the distance definition depends on the nature of the outcome (see Section 2.2.2 for the survival and competing risk settings). To improve accuracy and minimize the correlation between the trees, randomness is incorporated at each node  $d$  by considering only a random subset of candidate covariates  $\mathcal{M}^{(d)} = \{\mathcal{M}_x^{(d)}, \mathcal{M}_y^{(d)}\} \subset \{\mathcal{M}_x, \mathcal{M}_y\}$  which size is a tuning parameter, called *mtry*.

### 2.2.1 Internal processing for time-dependent covariates

For all the time-dependent covariates, a node-specific pre-processing is achieved to summarize the covariate dynamics into a set of time-independent features to be included in the pool of candidates for the splitting (see Figure 1(B)). At each node  $d$ , the trajectory of time-dependent covariate  $Y_m \in \mathcal{M}_y^{(d)}$  is modeled using a flexible mixed model<sup>21</sup> as:

$$Y_{ijm} = Z_{im}^T(t_{ijm})\beta_m^{(d)} + Z_{im}^T(t_{ijm})b_{im}^{(d)} + \epsilon_{ijm}^{(d)} \quad (1)$$

where  $Y_{ijm}$  is the covariate value for subject  $i$  at time  $t_{ijm}$ ,  $Z_{im}^T(t_{ijm})$  is the  $q_m$ -vector of functions of time associated with the fixed effects  $\beta_m^{(d)}$  and random effects  $b_{im}^{(d)}$  (with  $b_{im}^{(d)} \sim \mathcal{N}(0, B_m^{(d)})$ ).  $\epsilon_{ijm}^{(d)}$  denotes the error measurement with  $\epsilon_{ijm}^{(d)} \sim \mathcal{N}(0, \sigma_m^{2(d)})$ .

We present the method for continuous time-dependent covariates only. However, the pre-processing procedure could be easily adapted to other types of time-dependent covariates by replacing the linear mixed model in (1) by a generalized linear mixed model.

Any specification of the functions of time can be considered for  $Z_{im}^T(t_{ijm})$ . It has to be chosen carefully in preliminary analyses according to the repeated information available. To allow for a flexible modeling of the trajectory over time, we favor a basis of natural cubic splines with knots to be determined in input.

The maximum likelihood estimation of the parameters is performed at each node on the subset of subjects present at the node (i.e.  $\forall i \in S^{(d)}$ ). When the covariate has already been selected at a parent node, estimated parameters from the closest parent node are considered as initial values to drastically speed-up the procedure.

Time-independent features are then derived as the predicted individual deviations to the mean trajectory  $\mathbb{E}(Y_{im}(t)) = Z_{im}^T(t)\beta_m^{(d)}$ . Also known as the empirical Bayes estimates in the mixed model literature,<sup>21</sup> they are computed as the individual random-effect mean conditional to the individual data at the parameter estimates:

$$\begin{aligned}\hat{b}_{im}^{(d)} &= \mathbb{E}(b_{im}^{(d)} | Y_{im}) \\ &= \hat{B}_m^{(d)} Z_{im}^T \hat{V}_{im}^{-1(d)} (Y_{im} - \mathbb{E}(Y_{im})) \\ &= \hat{B}_m^{(d)} Z_{im}^T \hat{V}_{im}^{-1(d)} (Y_{im} - Z_{im} \hat{\beta}_m^{(d)})\end{aligned}\quad (2)$$

where  $Z_{im}$  is the matrix with  $j$ -row vectors  $Z_{im}^T(t_{ijm})$  (for  $j = 1, \dots, n_{im}$ ),  $\hat{V}_{im}^{(d)} = Z_{im} \hat{B}_m^{(d)} Z_{im}^T + \hat{\sigma}_{em}^{(d)} I_{n_i}$ ,  $I_{n_i}$  the  $n_i \times n_i$  identity matrix and the hat denotes the maximum likelihood estimates.

At this stage, the ensemble of candidate features for the time-dependent covariates becomes  $\mathcal{M}_{y\star}^{(d)} = \{\hat{b}_{im}^{(d)} \mid Y_m \in \mathcal{M}_y^{(d)}\}$  and the total ensemble of candidate features  $\mathcal{M}_{\star}^{(d)} = \{\mathcal{M}_x^{(d)}, \mathcal{M}_{y\star}^{(d)}\}$  is now only composed of time-independent features.

### 2.2.2 Splitting rule

At each node  $d \in \mathcal{D}$ , the subjects are to be split into the two daughter nodes that are the most different possible according to the outcome (Figure 1(D)). With a survival outcome, the difference is quantified according to the log-rank statistic. In the presence of competing risks, we used the Fine & Gray test statistic<sup>22</sup> because our objective is primarily the prediction of one of the events, and the Fine & Gray approach allows a more direct covariate assessment in that context compared to cause-specific models.<sup>23</sup> Nevertheless, other splitting rules could be used instead.<sup>19</sup>

The splitting procedure requires that each feature  $W \in \mathcal{M}_{\star}^{(d)}$  be dichotomized. For a continuous predictor, this is achieved by considering a dichotomization according to a threshold  $c$ :  $w_i > c$  or  $w_i \leq c$  with  $w_i$  indicating the individual value of  $W$  for subject  $i$ . We used each decile of  $W$  as a candidate threshold  $c$ . Alternatively  $c$  could be chosen according to values randomly drawn from  $W$ . For a non-continuous predictor, the dichotomization can be achieved as  $w_i \in c$  or  $w_i \notin c$  with  $c$  each possible subset of  $W$  modalities.

The log-rank test statistic with one cause or the Fine & Gray test statistic with multiple causes is computed for all potential dichotomized features (defined by couple  $\{W, c\}$ ), and the dichotomized feature  $(\{W_0^d, c_0^d\})$  that maximizes the test statistic is selected to create the left and right daughter nodes, denoted nodes  $2d$  and  $2d + 1$ , respectively.

### 2.2.3 Stopping criteria

Criteria need to be established to end the recursive procedure of a tree construction. We distinguish two criteria to pursue with the splitting of a node: (i) a minimum number of events called *minsplit*; (ii) a minimum number of subjects in each of the daughter nodes called *nodesize*. These two parameters that control the depth of the trees have to be tuned. Deeper trees are expected to give a lower error of prediction on the OOB sample and unravel more complex relationships between predictors and the outcome but they are also numerically more demanding. In our examples, we often used *nodesize* = 3 and *minsplit* = 5. This allowed for deep trees while ensuring that the mixed model and outcome model remained estimated on several individuals. When a stopping criterion is reached, the node is considered as a terminal node or leaf  $h \in \mathcal{H}$ .

### 2.2.4 Leaf summary

The subjects classified in the same leaf are supposed to be homogeneous in terms of their probability of event of interest. Each leaf  $h^b$  of tree  $b$  is thus summarized by the cumulative incidence function (CIF) for cause  $k$  ( $k = 1, \dots, K$ ):

$$\pi_k^{h^b}(t) = P(T_i < t, \delta_i = k \mid i \in h^b), \quad \forall t \in \mathbb{R}^+ \quad (3)$$

An estimate  $\hat{\pi}_k^{h^b}(t)$  of the CIF  $\pi_k^{h^b}(t)$  is given by the Aalen–Johansen estimator.

## 2.3 Individual prediction of the outcome

### 2.3.1 OOB individual prediction

Let us consider an individual  $\star$  with the  $P$ -vector of time-independent covariates  $X_\star$ , and the ensemble of time-dependent covariate observations  $\mathcal{Y}_\star = \{Y_{\star jm}, m = 1, \dots, Q, j = 1 \dots n_{\star m}\}$ . The individual-specific CIF for individual  $\star$  in tree  $b$  is given by:

$$\begin{aligned}\pi_{\star k}^b(t) &= P(T_\star < t, \delta_\star = k \mid \mathcal{Y}_\star, X_\star, b) \\ &= P(T_\star < t, \delta_\star = k \mid \star \in h_\star^b) \\ &= \pi_k^{h_\star^b}(t)\end{aligned}\quad (4)$$

where  $h_\star^b$  is the leaf in which individual  $\star$  ends when dropping into tree  $b$ . Specifically, at each node  $d$ , subject  $\star$  is recursively assigned to the left or right node according to whether  $w_\star^d > c_0^d$  or  $w_\star^d \leq c_0^d$ . In the case where  $W_0^d$  is a predicted random-effect from time-dependent covariate  $m$ , the random-effect prediction for individual  $\star$ ,  $\hat{b}_{\star m}^{(d)}$ , is computed using formula (2) with the estimated parameters obtained at this specific node  $d$ .

An ensemble estimate of the individual CIF  $\hat{\pi}_{\star k}(t)$  for cause  $k$  can finally be defined by aggregating the tree-specific individual predictions  $\hat{\pi}_{\star k}^b(t) = \hat{\pi}_k^{h_\star^b}(t)$  over all the trees  $\mathcal{O}_\star \subset \{1, \dots, B\}$  for which  $\star$  is *OOB*, as:

$$\hat{\pi}_{\star k}(t) = \frac{1}{|\mathcal{O}_\star|} \sum_{b \in \mathcal{O}_\star} \hat{\pi}_k^{h_\star^b}(t) \quad (5)$$

where  $|\mathcal{O}_\star|$  denotes the length of  $\mathcal{O}_\star$  and  $\hat{\pi}_k^{h_\star^b}(t)$  is the Aalen–Johansen estimator in leaf  $h_\star^b$  of the  $b$ -th tree.

### 2.3.2 Individual dynamic prediction from a landmark time

The methodology described in the previous section for an OOB individual can be used to provide the individual dynamic prediction of the outcome of cause  $k$  from the information collected up to a landmark time  $s$ . Let's consider a new subject  $\star$  still at risk of the event at time  $s$ . The covariate information available at the time of prediction is the  $P$ -vector of time independent covariates  $X_\star$  and the history of time-dependent covariates observations up to time  $s$ ,  $\mathcal{Y}_\star(s) = \{Y_{\star jm}, m = 1, \dots, Q, j = 1, \dots, n_{\star m}, t_{\star jm} < s\}$ . The probability of experiencing cause  $k$  of event at a horizon time  $w$  is then defined as:

$$\begin{aligned}\pi_{\star k}(s, w) &= P(s < T_\star \leq s + w, \delta_\star = k \mid T_\star > s, \mathcal{Y}_\star(s), X_\star) \\ &= \frac{\pi_{\star k}(s + w) - \pi_{\star k}(s)}{1 - \sum_{l=1}^K \pi_{\star l}(s)}\end{aligned}\quad (6)$$

where each  $\pi_{\star k}(t)$  (for  $k = 1, \dots, K$ ) can be estimated using equation (5) with the history of the time-dependent covariates  $\mathcal{Y}_\star(s)$  up to the landmark time  $s$  only, and  $\mathcal{O}_\star = \{1, \dots, B\}$ .

## 2.4 Error of prediction

The error of prediction can be used in RSF with two objectives: (i) tuning the hyper-parameters of the RSF (*mtry*, *minsplit*, and *nodesize*) to achieve an optimal RSF. This is done by minimizing the OOB error of prediction; (ii) assessing the predictive performances of the optimal RSF. This is achieved by computing the error of prediction for an external validation sample, that is a sample where subjects are OOB for all the trees. In this work, we considered mainly the Brier Score measure with an estimator adapted to the competing risk setting,<sup>24</sup> and its integrated version (IBS) between two time points  $\tau_1$  and  $\tau_2$  to assess the error of prediction.

### 2.4.1 IBS for optimizing the RSF

For the optimization of the RSF, the IBS estimator is given by  $IBS(\tau_1; \tau_2) = \int_{\tau_1}^{\tau_2} \hat{BS}(t) dt$  with the Brier Score estimated by:

$$\hat{BS}(t) = \frac{1}{N} \sum_{i=1}^N \hat{\omega}_i(t) \left\{ I\left(\tilde{T}_i \leq t, \delta_i = k\right) - \hat{\pi}_{ik}(t) \right\}^2 \quad (7)$$

where  $\hat{\pi}_{ik}(t)$  is the estimated probability of event of cause  $k$  given  $Y_i$  and  $X_i$  defined in (5), and  $\hat{\omega}_i(t)$  are inverse probability of censoring weights (IPCWs) that account for the censoring between  $\tau_1$  and  $\tau_2$ .<sup>25</sup> Following Blanche et al.,<sup>24</sup> we computed the IPCW using the Kaplan–Meier estimator of the censoring time survival function.

By default,  $(\tau_1, \tau_2)$  corresponds to the span of the time to event data, with  $\tau_1 = 0$  and  $\tau_2 = \max_{i \in \{1, \dots, N\}} \tilde{T}_i$ .

#### 2.4.2 External assessment of RSF predictive performances

For the external evaluation of the RSF performances, the IBS computation slightly differs. First, it is now computed on an external sample of size  $N^*$ , and the information considered is now the information up to the prediction time  $s$ , with  $s \leq \tau_1$ , so that  $\hat{IBS}^s(\tau_1; \tau_2) = \int_{\tau_1}^{\tau_2} \hat{BS}^s(t) dt$  with:

$$\hat{BS}^s(t) = \frac{1}{N^*} \sum_{\star=1}^{N^*} \hat{\omega}_{\star}^s(t) \left\{ I\left(\tilde{T}_{\star} \leq t, \delta_i = k\right) - \hat{\pi}_{\star k}(s, t-s) \right\}^2 \quad (8)$$

where  $\hat{\pi}_{\star k}(s, t-s)$  is the estimated probability of event of cause  $k$  between  $s$  and  $t$  given the information on  $Y_{\star}$  and  $X_{\star}$  up to  $s$  (see definition in (6)), and  $\hat{\omega}_{\star}^s(t) = \hat{\omega}_{\star}(t)I(\tilde{T}_{\star} > s)$ .

In the absence of an external sample (as in the application), the evaluation of the RSF performances can be incorporated into a K-fold cross-validation strategy: the random forest is built on  $K-1$  folds and dynamic predictions (considering data up to  $s$  only) are computed on the left-out fold. By replicating this on all the folds, estimated probabilities  $\hat{\pi}_{\star k}(s, t-s)$  of event between  $s$  and  $t$  are finally obtained for the entire sample and the Brier Score can be computed according to equation (8). This strategy was adopted in the application and repeated 50 times to account for the 10-fold cross-validation variability.

## 2.5 Importance of the predictors

Beyond the overall predictive performance of the approach, one can be interested in identifying which predictors are the most predictive. We propose to evaluate the association between event and predictors through two measures: the variable importance (VIMP) and the minimal depth.

#### 2.5.1 Variable importance

The VIMP measures the variable prediction ability by computing the increase in OOB error obtained after breaking the link between a given variable and the event. Such a link is broken by permuting the values of variable  $p$  across individuals when  $p$  is time-fixed and across observations when  $p$  is time-dependent (i.e. for time-dependent variables, values for all individuals at all time points are permuted all together). Then, the VIMP statistic for covariate  $p$ , called  $VIMP^{(p)}$ , is the difference between the mean over the trees of OOB errors obtained after permuting the values of covariate  $p$  ( $\hat{IBS}_b(\tau_1, \tau_2)^{(p)}$ ) for  $b = 1, \dots, B$ ) and the mean over the trees of the OOB errors ( $\hat{IBS}_b(\tau_1, \tau_2)$ ) for  $b = 1, \dots, B$ ):

$$VIMP^{(p)}(\tau_1, \tau_2) = \frac{1}{B} \sum_{b=1}^B \hat{IBS}_b(\tau_1, \tau_2)^{(p)} - \frac{1}{B} \sum_{b=1}^B \hat{IBS}_b(\tau_1, \tau_2) \quad (9)$$

where  $\hat{IBS}_b(\tau_1, \tau_2)^{(p)}$  and  $\hat{IBS}_b(\tau_1, \tau_2)$  are defined similarly as the IBS by computing the Brier Score (in equation (7)) only on  $b$ -tree OOB subjects and using the estimate of  $b$ -tree individual prediction  $\hat{\pi}_{k^*}^{h^b}(t)$  defined under equation (5).

Large VIMP value indicates a loss of predictive ability when removing covariate  $p$ , whereas null VIMP value indicates no predictive ability. Due to the permutation procedure, negative VIMP may be obtained. They are interpreted as null VIMP.

#### 2.5.2 Grouped VIMP

Because of the potential correlation between variables, the VIMP computed at the variable level may not always indicate the correct variable-specific predictive ability. To assess the predictive ability of correlated variables, Gregorutti et al.<sup>26</sup> proposed the grouped VIMP (gVIMP) statistic in standard random forest. It consists in simultaneously noising-up all the variables of a given group. We considered the same methodology for our RSF. The overall gVIMP statistic for group  $g \in \{1, \dots, G\}$  is defined as  $gVIMP^{(g)} = \frac{1}{B} \sum_{b=1}^B \hat{IBS}_b^{(g)} - \frac{1}{B} \sum_{b=1}^B \hat{IBS}_b$ , where  $\hat{IBS}_b^{(g)}$  denotes the OOB error obtained when noising-up all the variables from group  $g$ .

### 2.5.3 Average minimal depth

The minimal depth of a variable in a tree corresponds to the distance between the root node and the first node that used the variable for splitting the data. The minimal depth can be averaged across all the trees allowing to rank the predictors. Indeed, during the tree building, the most predictive variables are expected to be chosen for the first splits so the closer the average minimal depth from one, the better the predictive ability of the variable. When only a random subset of variables are considered at each node ( $mtry < P + Q$ ), the interpretation of the minimal depth may be blurred. We thus recommend to compute this statistic only for the maximal  $mtry = P + Q$ . Moreover, because the depth of the trees may vary and some predictors may not be systematically used in the tree building process, we recommend to report the number of trees where the predictor was selected along with the average minimal depth. Note that, compared to the VIMP, the minimal depth can be computed both at the summary feature and at the covariate level thus providing complementary information about the tree building process. However, the minimal depth is likely sensitive to the number of possible splits of a covariate and may in particular lead to larger minimal depth for binary variables compared to others.

## 3 Simulation study

We carried out a simulation study to illustrate the behaviour of DynForest in comparison with alternative methods under two types of scenarios:

- **Sm** (for small): repeated data of two longitudinal predictors. We compared the performances of DynForest with a JM estimated using JMBayes R package.<sup>11</sup> For JMBayes, we considered the same specification for the linear mixed models as in DynForest and modeled the association with the event with a proportional hazard model (baseline risk function approximated by four cubic splines) that included the current levels and current slopes of the two predictors as covariates.
- **La** (for large): repeated data of 20 longitudinal predictors. We could not compare with a JM anymore. Instead, we compared DynForest with a RC technique in which the exact same specification for the linear mixed models and the exact same strategy for the RSF were considered. The difference in the RC was that the linear mixed models were estimated once and for all prior to the application of standard RSF.

For both scenarios Sm and La, we additionally included two time-fixed predictors unrelated to the event. Finally, we compared the predictive performance of the techniques in predicting the clinical event occurrence at two horizon times  $w = 1, 2$  or  $w = 2, 3$  from two landmark times  $s = 2, 4$  or  $s = 2, 5$ . We measured the performance with both Brier Score (defined in (7)) and area under the ROC curve (AUC) with estimators adapted to dynamic prediction.<sup>24</sup>

### 3.1 Design

For all scenarios,  $R = 250$  samples of  $N = 500$  individuals were built for the learning step and a single external validation sample of  $N = 500$  individuals was generated for evaluating the predictive performance.

For each subject, we generated two time-fixed covariates (one continuous according to a standard Gaussian distribution and one binary according to a Bernoulli with probability 0.5). We also generated repeated data of 2 or 20 continuous time-dependent predictors, for small and large dimension scenarios, respectively. Times of measurement were at baseline and then randomly drawn (using an exponential departure) around theoretical annual visits up to 10 years. Six scenarios were considered for the small dimension (Sm1 to Sm6). Sm1 corresponded to a well-specified JM with each marker generated according to a linear-trajectory mixed model and an association with the event through the current level of marker 1. For all the other scenarios, each marker trajectory followed a latent class linear mixed model<sup>27</sup> with four classes and either class-specific linear individual trajectories or class-specific nonlinear individual trajectories approximated with natural cubic splines. The risk of event was then generated using a proportional hazard model with a Weibull baseline hazard with shape and scale parameters equal to 0.1 and 2, respectively. Independent censoring was modeled using an exponential risk. In scenarios Sm2 and La2, the association with the event was through the latent class membership. For scenarios Sm3 to Sm6 and La1, the association was through the marker-specific random-effects and possibly two-by-two interactions between random-effects. Scenarios Sm5 and Sm6 were variations of Sm3 with non-proportional hazard (Sm5) and covariate-dependent censoring (Sm6). The generation procedure is fully detailed in Supplemental Materials with section “Simulations” describing the data generation, Supplemental Table S1 summarizing the scenarios characteristics, and Supplemental Tables S2 and S3 reporting the generating parameters. Individual trajectories of scenarios Sm2 to Sm6 are also displayed in Supplemental Figure S1.

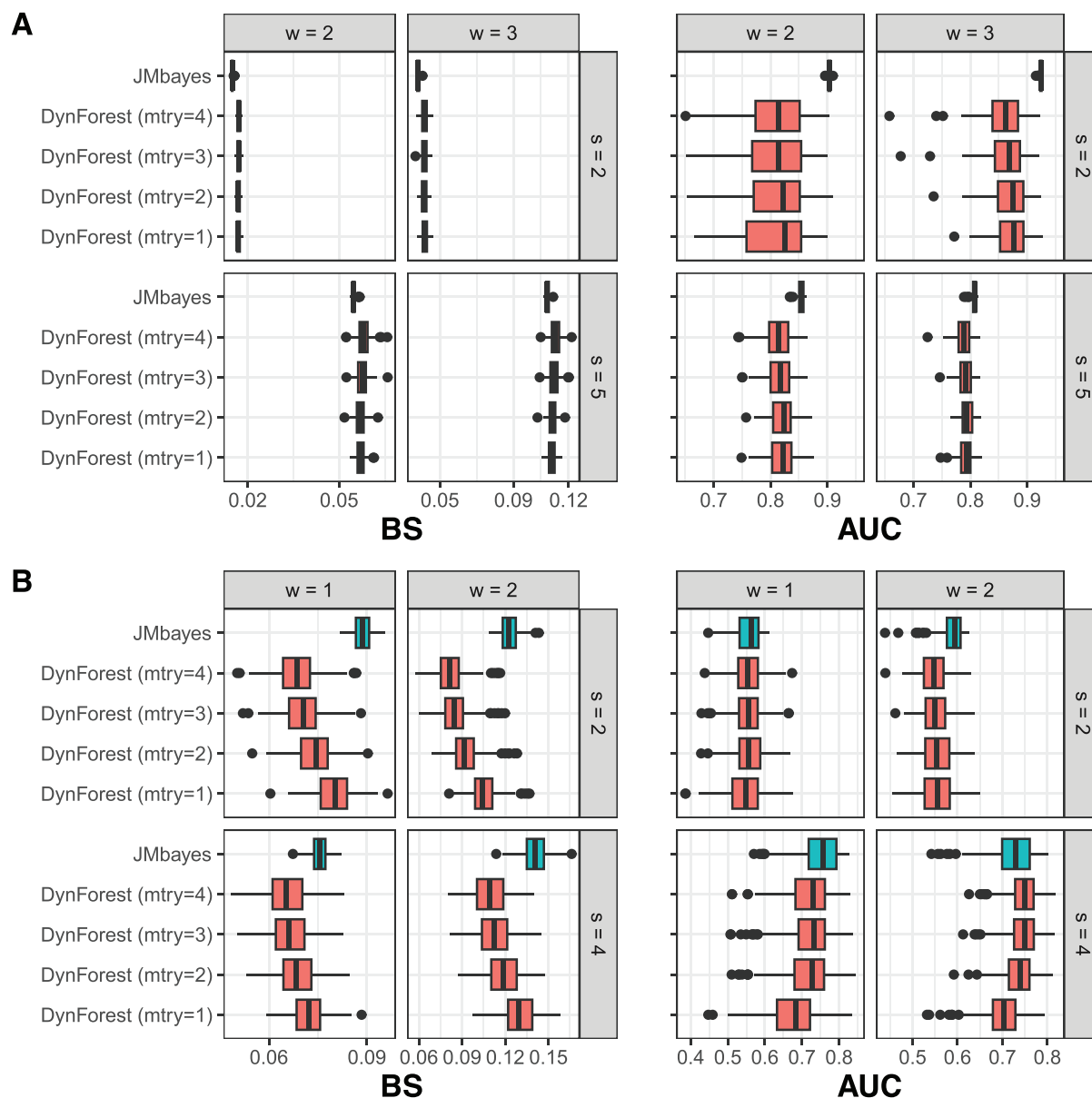


**Figure 2.** External predictive performances of DynForest and JMBayes in small dimension scenarios (with two time-dependent predictors) Sm1 (panel A) and Sm2 (panel B) for the 250 replications. Are reported the Brier Score (BS) and the area under the ROC curve (AUC) at two landmark times  $s = 2, 5$  and two horizons  $w = 2, 3$  for scenario Sm1, and  $s = 2, 4$  and  $w = 1, 2$  for scenario Sm2. JMBayes is correctly specified in Sm1 and incorrectly specified in Sm2. For DynForest, we fixed  $nodesize = 3$  and  $minsplit = 5$ , and their results are reported for all  $mtry$  values to underline the importance of this tuning parameter.

## 3.2 Results

### 3.2.1 Small dimension scenarios

Predictive performances on the external dataset are reported in terms of BS and AUC in Figure 2 for scenarios Sm1 and Sm2, and in Supplemental Figures S2 to S5 for scenarios Sm3 to Sm6. For DynForest, we fixed  $nodesize = 3$  and  $minsplit = 5$  to favor deep trees and reported the results with each possible value of  $mtry$  to underline the importance of this tuning parameter. As expected, the results varied substantially according to its value. The best performances in terms of BS (minimal BS) was systematically obtained with the largest  $mtry$ , that is four (two time-dependent and two time-fixed predictors), and the worst with  $mtry = 1$ . For the AUC, the differences were less visible.

In scenario Sm1, as expected, the well-specified JM performed slightly better (lower BS and higher AUC) compared to DynForest approach. In the other scenarios Sm2 to Sm6 in which JM was misspecified (due to the mixture of trajectory



distributions and different types of association with the event), DynForest showed lower Brier Score. For the AUC, the results were more nuanced depending on the scenarios. Regarding the covariate importance, VIMPs of scenarios Sm1 and Sm3 (Supplemental Figure S7) confirm that DynForest correctly retrieved the markers associated with the event.

This first simulation study shows that, even in a small dimension setting where JM can be estimated, DynForest constitutes a competing alternative to JM for individual dynamic prediction purpose since it does not rely on stringent assumptions and can thus handle more complex data and association structures.

### 3.2.2 Large dimension scenarios

In the large dimension scenarios La1 and La2, we report in Figure 3, the predictive performances on the external dataset of DynForest and its RC counterpart (or two-stage counterpart). For both techniques, we fixed *nodesize* = 3 and *minsplit* = 5. For *mtry* parameter, the range of possible values was 1–22 for DynForest and 1–62 for the RC method. Since tuning this parameter on each dataset would be computationally too intensive, we tuned it on the first replication only and used this value for all the replications. With nonlinear association using random-effects plus interactions, optimal values were *mtry* = 9 and *mtry* = 46 for DynForest and RC, respectively. They were *mtry* = 5 and *mtry* = 6 when linking the markers to the event through the latent class membership. DynForest outperformed the RC technique for both BS and AUC with nonlinear association using latent class membership (La2, Figure 3(B)). Under nonlinear association using random-effects with interactions (La1, Figure 3(A)), the results were still slightly in favor of DynForest. Because of the critical role *mtry* may have on the results, we ran additional simulations to assess the impact of not tuning *mtry* on each replicate on 100 replications of scenario La2 (Supplemental Figure S6). The final performances between the tuned and untuned versions were very close, with exception for the AUC of RC at landmark time 2.

This second set of simulations underlined the substantial impact of not including the time-dependent predictor modeling step within the survival tool construction to correctly account for the correlation between the longitudinal and survival processes and informative dropout.

Along with predictive abilities, variable importance, and *mtry* critical role, we also explored the calibration of predictions stemmed from DynForest. As shown in Supplemental Figures S8 and S9 for scenarios Sm5 and La1, predictions were overall calibrated across replications.

## 4 Application

We aimed at predicting the individual probability of dementia in the elderly in the presence of competing death by leveraging the history of repeated data on clinical exam, neuropsychological battery and brain MRI exam. We relied for this on the Three-City (3C) cohort study.<sup>28</sup>

### 4.1 The 3C study

The 3C study is a French prospective population-based cohort study which enrolled individuals aged 65 years and older from electoral rolls in three French cities (Bordeaux, Dijon, and Montpellier). Extensive follow-up interviews were conducted at baseline and then two, four, seven, 10, 12, 14, and 17 years after the enrollment including an extensive clinical and neuropsychological exam done in-person at home by a trained psychologist. At one, four, and 10 years, a subsample underwent an additional MRI exam. The diagnosis of dementia relied on a two-step procedure with suspected cases of dementia examined by a clinician and validated by an independent expert committee of neurologists and geriatricians. Deaths were continuously recorded but were considered as a competing event for dementia only in the three years after a negative diagnosis. Our analytical sample included all the individuals free of dementia at baseline and with at least one measure at each of the 29 predictors under study during the follow-up in Bordeaux and Dijon cities. This led to a sample of  $N = 2140$  subjects (with 10,766 observations) among which 234 were diagnosed with an incident dementia and 311 died before any dementia (Supplemental Figure S14).

We considered a total of 24 time-dependent and five time-fixed predictors structured into nine groups: socio-demographic (time-fixed age at baseline, education, and gender), cardio-metabolic factors (three time-dependent markers with body mass index, diastolic and systolic blood pressure, and one time-fixed with diabetes status at baseline), medication (time-dependent number of medication), depressive symptomatology (one time-dependent scale of depressive symptomatology), cognition (four time-dependent cognitive tests), functional dependency (one time-dependent scale of instrumental activities of daily living), genetic (time-fixed APOE4 allele carrier status), neurodegeneration (eight time-dependent brain MRI markers including regional volumes and global measures), and vascular brain lesions (six time-dependent markers of white matter hyperintensities). Complete information on the predictors are provided in Supplemental Tables S4 to S9. For longitudinal predictors, individual trajectories are displayed in Supplemental Figures S11 to S13.

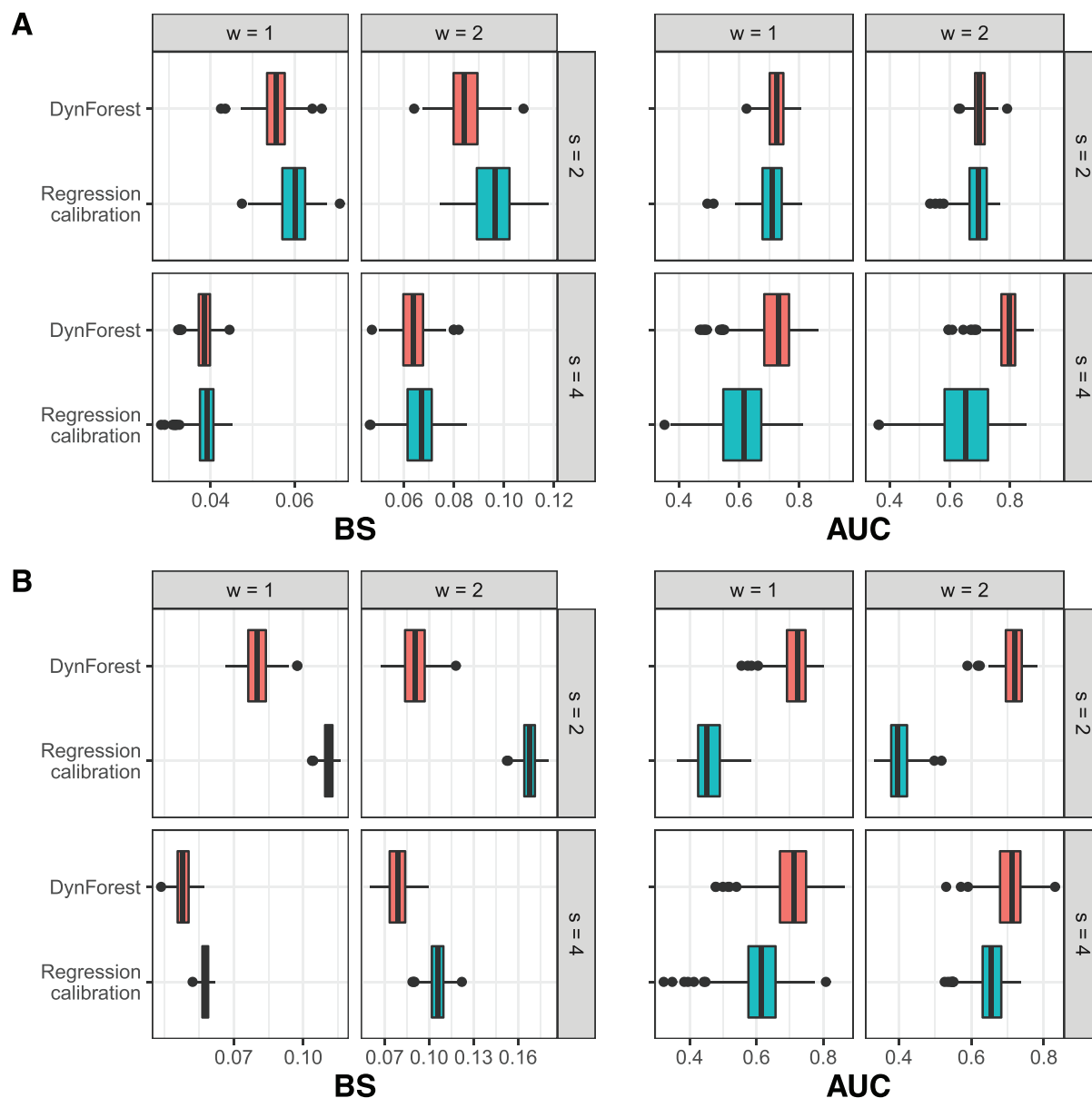


**Figure 3.** External predictive performances of DynForest and its regression calibration version in the large dimension scenario of simulations (20 predictors) for the 250 replications. Are reported the Brier Score (BS) and the area under the ROC curve (AUC) at two landmark times  $s = 2, 4$  and two horizons  $w = 1, 2$ . Nonlinear association between the markers and the event was displayed using random-effects with two-by-two interactions (A) or latent class membership (B). The regression calibration version of DynForest consisted in summarizing the time-dependent markers into time-fixed features once for all prior to inclusion in the RSF. We fixed  $nodesize = 3$  and  $minsplit = 5$ .  $mtry$  parameter was also fixed for all replications after tuning process on an unique dataset.

## 4.2 DynForest specification

The probability of dementia was predicted according to time from the enrollment. MRI data were collected 1.7 times on average and modeled using quadratic and linear trajectories at the population and at the individual level, respectively. Other time-dependent predictors were measured 5.1 times on average. Their trajectories according to time in the study were modeled in the main analysis using natural splines with one internal knot both at the population and individual levels. To satisfy the normality assumption of the linear mixed model, all time-dependent predictors were previously normalized using splines transformations.<sup>29</sup>

In the absence of an external dataset available with the same longitudinal predictors and the same target population, predictive abilities were assessed using a 10-fold cross-validation procedure to avoid over-fitting. For each of the 10 folds,

DynForest was trained on the sample that excluded the fold (learning step on 90%) and individual probabilities of dementia were computed on the fold (prediction step on the remaining 10%). The cross-validation procedure was repeated  $R = 50$  times to appreciate the variability of the results. During the learning step, we systematically fixed parameters  $minsplit = 5$  and  $nodesize = 3$  to favor deep trees. The  $mtry$  parameter was tuned within the range of possible value (from 1 to 29 predictors) to minimize the OOB IBS. On the total sample, we first observed that the OOB IBS decreased rapidly with increasing  $mtry$  until a stabilization around  $mtry = 15$  (Supplemental Figure S15). So for each fold, we ran DynForest twice with  $mtry = 15$  and  $mtry = 20$  and selected the optimal  $mtry$  according to the OOB IBS. For the prediction step, individual dementia probabilities were computed for the remaining fold following (5).

### 4.3 Results

To better understand the importance of each predictor, we report the VIMP statistics in Figure 4(A). The VIMP statistics were computed 10 times and averaged across the replications to reduce the variability due to the permutation procedure. IADL (functional dependency) was the marker the most associated to dementia with a mean gain in IBS of 4.5%, followed by neuro-degeneration markers with the right hippocampus and lobe medio-temporal volumes (gains of 4.2% and 3.1%, respectively), and cognitive tests with the Isaacs Set test and Benton test (gains of 3.4% and 2.6%, respectively). Since the VIMP may not correctly translate the importance of correlated variables, we also reported in Figure 4(B) the gVIMP grouped by dimensions. The eight neuro-degeneration predictors reached a mean gain of 10.3% of IBS, and the four cognitive tests a mean gain of 9.2%. Then, we observed less importance for the unique marker of functional dependency (mean gain of 4.5%) followed by the six markers of vascular brain lesions (mean gain of 3.6%).

We also computed the minimal depth when using the largest  $mtry$  hyper-parameter (i.e.  $mtry = 29$ ) (Figure 5). IADL (functional dependency) and cognition tests (Isaacs Set test, Benton test, and Trail Making Test A) were the predictors with the lowest average minimal depth, and were selected 100%, 100%, 98%, and 97% among the trees, respectively. It means that these predictors were the most effective to split the individuals into homogeneous subgroups according to their risk difference. Except for Trail Making Test A, these results were in accordance with those obtained using the VIMP statistic. It should be noted that the minimal depth may be sensitive to the nature of the covariates. In our example, the three binary variables (gender, ApoE4 status, and diabetes status) were the covariates appearing with the lowest frequency although the minimal depth remained comparable with those of the other covariates.

We then considered two landmark times  $s = 5, 10$  years to assess the predictive abilities of DynForest to predict dementia between  $s$  and  $s + w$  (horizon times  $w = 3, 5$  years) from individual history up to time  $s$ . This resulted in 1727 and 1150 individuals still at risk of dementia, respectively. The cross-validated AUC and BS (Figure 6) varied from 0.78 to 0.80 and from 0.048 to 0.086 depending on the landmark and the horizon times. For comparison, we also reported in Figure 6, the predictive ability measures when considering more restrictive linear trajectories for all the markers, the predictive ability were generally worse (larger BS and lower AUC).

We finally explored the predictive ability of each predictor in this landmark context by computing the VIMP and gVIMP using only the information prior to five years and considering a short span from five to 10 years (Supplemental Figure S16). Again, IADL had the largest VIMP value, followed by the Isaacs Set test and the right hippocampus volume.

## 5 Discussion

We developed an original methodology, called DynForest, to compute individual dynamic predictions from multiple longitudinal predictors. We extended the RSF (which were limited so far to time-fixed predictors)<sup>19,20</sup> to handle endogenous longitudinal predictors. This was achieved by including in the tree building a node-specific internal processing to translate the longitudinal predictors into time-fixed features. DynForest can be used to compute individual dynamic predictions of events as well as quantify the importance of the longitudinal predictors using VIMP and grouped-VIMP adapted to longitudinal data.

Through a simulation study, we first showed in a small dimensional context that DynForest could be a relevant alternative to the JM reference technique. Indeed, in contrast with JM, DynForest does not need to pre-specify the association structure with the event, and may account for nonlinear associations and interactions. In the second scenario, we considered a larger dimensional context, with 20 longitudinal markers, for which JM could not be estimated anymore. We showed, in this larger dimensional scenario, that DynForest outperformed the RC alternative proposed in the literature.<sup>14,16,17</sup> Indeed, in contrast with RC technique, DynForest accounts for the truncation of the repeated data due to the event by re-estimating the mixed models at each node on the node-specific subsample. Since these subsamples become more and more homogeneous regarding the event, the missing at random assumption of the mixed models becomes more and more valid.

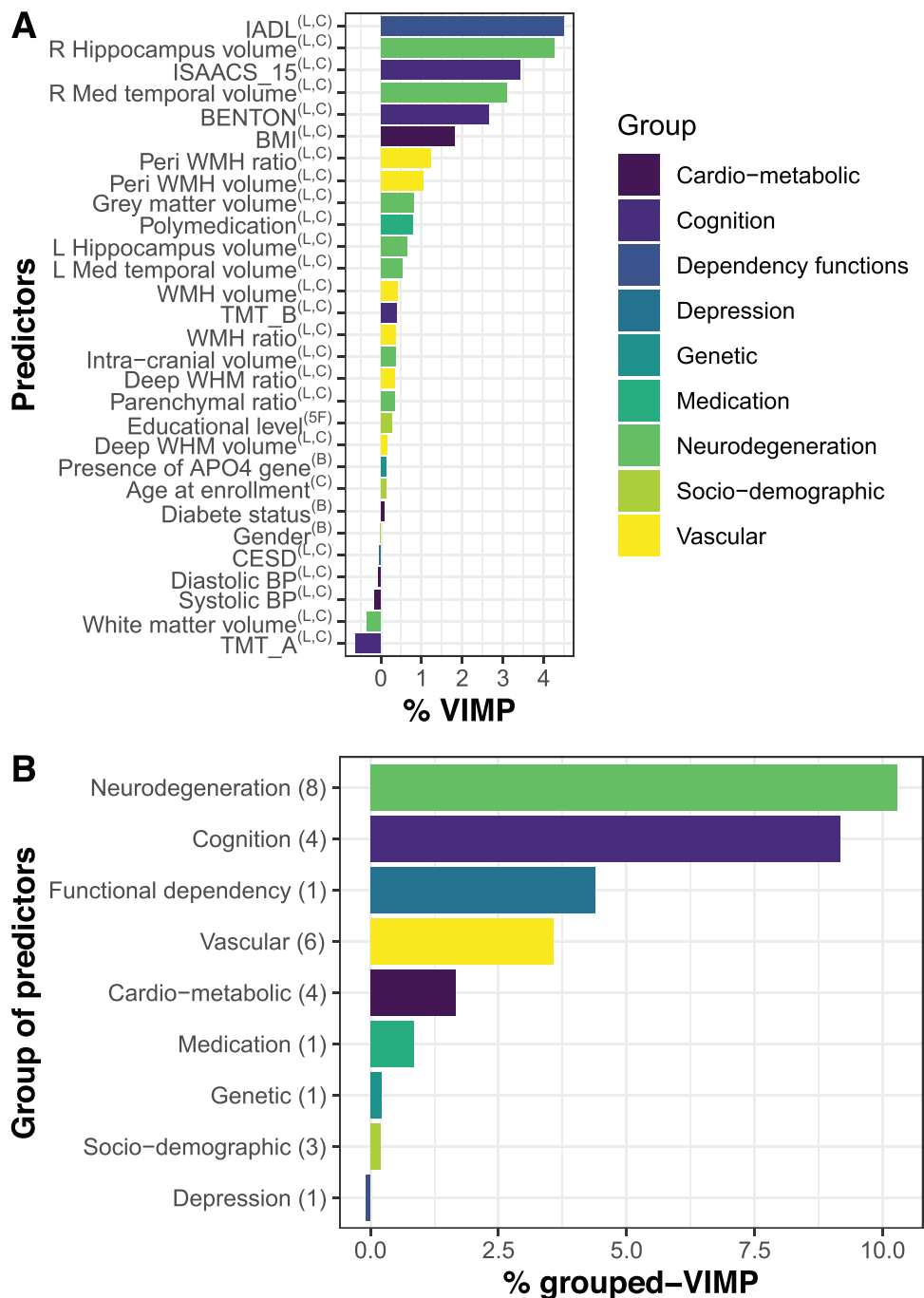


**Figure 4.** (A) Importance variable (VIMP) and (B) grouped importance variable (gVIMP) averaged over 10 permutation procedures for each dementia predictor or group of dementia predictors. Application in the 3C study. The nature of each predictor is reported with (L, C) for continuous longitudinal, (B) for time-fixed binary, (C) for time-fixed continuous and (5F) for time-fixed categorical with five levels.

Compared with the other methodologies adapted to the large dimensional and longitudinal context, our methodology has the assets of (i) using all available information when landmark approaches<sup>8,9</sup> only include subjects still at risk at landmark time, resulting in a lack of efficiency<sup>7</sup>; (ii) simultaneously analyzing the longitudinal and time-to-event processes when the other methods based on two-step RC<sup>14,16,17</sup> neglect the association leading to a potential bias in the prediction; (iii) allowing for complex and nonlinear association structures between the predictors and the event; (iv) allowing the analysis of potentially high-dimensional data (i.e. hundreds/thousands of predictors). Indeed, the longitudinal markers are

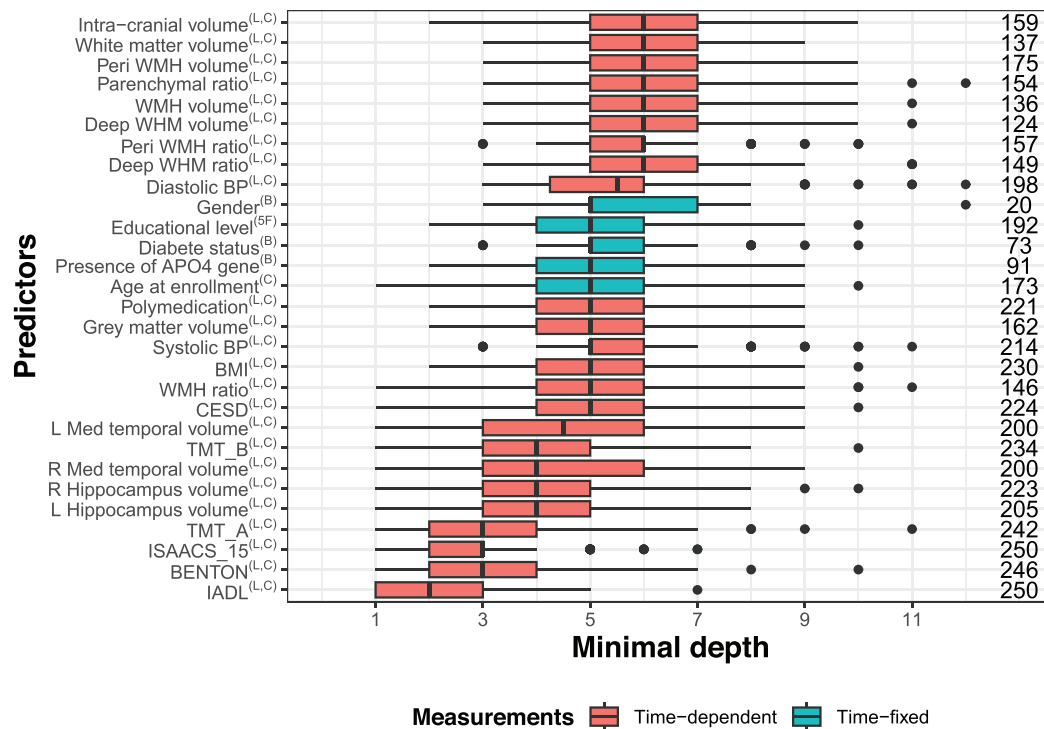


**Figure 5.** (A) Minimal depth computed with the largest *mtry* hyper-parameter (i.e. *mtry* = 29) for each predictor of dementia. We display on the right of the graph the amount of tree where the predictor is found among the 250 trees used to build the random forest. The nature of each predictor is reported with (L, C) for continuous longitudinal, (B) for time-fixed binary, (C) for time-fixed continuous and (5F) for time-fixed categorical with five levels.

independently modeled so that the method could be easily applied no matter the number of longitudinal markers. Finally, we introduced two stopping criteria defining the minimum number of events and of subjects required to proceed to a subsequent split. This allows some leaves to have a homogeneous subsample with no events.

Our methodology has also drawbacks. First, although it may be applied whatever the number of predictors, the computation time may become extremely long in high-dimensional settings, in particular with a large number of candidates *mtry*. Indeed, mixed models are to be estimated at each node of each tree even though we managed to fasten the estimation by using the estimates previously obtained as initial values. As an example, we report the computation time of replicates in simulation scenario La1 with 20 time-dependent covariates in Supplemental Figure S10. Second, we analyzed continuous longitudinal markers only. Other natures of repeated markers (e.g. binary, categorical, and counts) could be considered using generalized mixed models. Third, we rely on the same assumptions as the splitting rule. By using the log-rank and Fine & Gray statistics, the methodology may miss covariates associated with survival curves or cumulative incidences that cross over time. We also assume an independent censoring within each node. However, since the nodes are becoming more and more homogeneous regarding covariate profiles as the trees are growing, the independence censoring assumption in each node is likely to be more and more valid. We note that the splitting rules (Log-rank statistic or Fine & Gray statistic) are only used to rank the features, not to quantify the association. Fourth, we relied on linear mixed models for deriving time-fixed features. Functional principal components analysis<sup>13</sup> could be considered instead. We leave such development for future research. The mixed models account for the sparse and irregular measurement timings and they are robust to missing at random data. However, they only focus on the marker level and they require the pre-specification of the time functions defining the overall shape of marker trajectory. We assumed a different specification across markers but the same specification across all the nodes of a marker. The time functions should be carefully chosen in preliminary analyses as a balance between flexibility and amount of available information. For instance, in the application, since only two to three measures were available for MRI-derived markers, we constrained the number of random effects to two for these markers. In contrast, flexible splines functions were considered for the other markers that were more frequently measured. Furthermore, as mixed models require an estimation, convergence issues may arise times to times. In the case where convergence is not reached for a marker at a node, we decided to remove the marker from the potential splits of this node. Another option would be to compute the random-effects at the last iteration of the optimization algorithm even when the algorithm

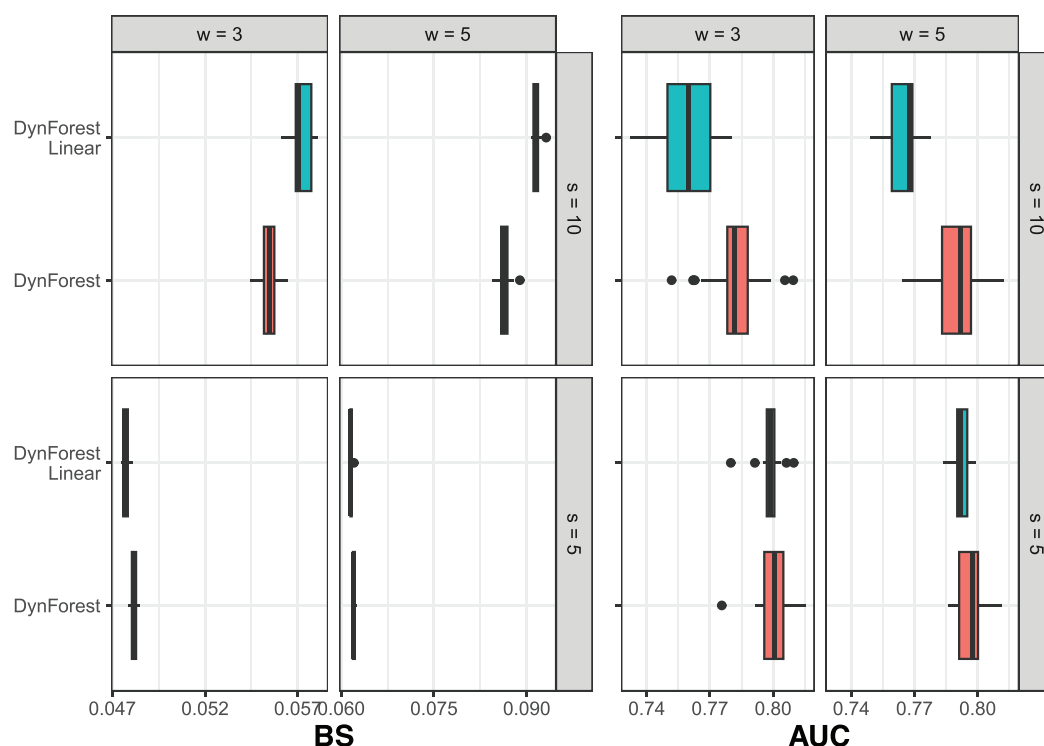


**Figure 6.** Predictive assessment of dementia at landmark times  $s = 5, 10$  years and horizon times  $w = 3, 5$  years using Brier Score (BS) and area under the ROC curve (AUC) in the 3C study for two specifications. In DynForest, trajectories of time-dependent markers from cardio-metabolic, medication, depressive symptomatology, cognition, and functional dependency were modeled using natural cubic splines. In DynForest-Linear, we modeled them as linear trajectories.

has not converged yet. As shown in Supplemental Figure S17, convergence issues rarely occurred in the application. The most impacted markers were those stemmed from brain MRI with a proportion of non-convergence that did not exceed 5% of the total number of nodes, and occurred mostly from node depth four. For the other markers, convergence issues almost never occurred. The last drawback of the methodology concerns the quantification of the strength of the association between the predictors and the event. The VIMP and gVIMP statistics do not inform on the sign or the structure of the association. Instead they quantify the added predictive ability of specific markers or of groups of markers. This may be particularly useful in prediction tool development for instance to evaluate the value of carrying out expensive exams (such as MRI in our context) or invasive exams.

To conclude, using the framework of the random survival forests combined with mixed models for internally processing longitudinal predictors, we tackled the challenge of predicting an event from a potential high number of longitudinal endogenous predictors. In the methodology building process, we had to make many choices (e.g. regarding the splitting rules, the stopping criteria, the use of linear mixed models for the time-dependent predictors, and the use of IBS for OOB evaluation). We leave to future research the exploration of such additional features. In the meantime, DynForest already offers an innovative solution accompanied by a user-friendly R package.

### Acknowledgements

We thank Dr Carole Dufouil (University of Bordeaux, Inserm) for providing 3C data Dijon center, and Dr Louis Capitaine for FrechForest R code used in DynForest.

### Declaration of conflicting interests

The author(s) declared no potential conflicts of interest with respect to the research, authorship and/or publication of this article.

### Funding


The author(s) disclosed receipt of the following financial support for the research, authorship, and/or publication of this article: This work was funded by the French National Research Agency (ANR-18-CE36-0004 for project DyMES), and the French government in


the framework of the PIA3 (“Investment for the future”) (project reference 17-EURE-0019) and in the framework of the University of Bordeaux’s IdEx “Investments for the Future” program / RRI PHDS.

## Software

DynForest R package is available on CRAN and on GitHub at <https://github.com/anthonydevaux/DynForest>. Replications scripts for simulation are available on GitHub at <https://github.com/anthonydevaux/dynforest/paper/supp>. The application data are available on specific request to the steering committee of the 3C study.

## ORCID iDs

Anthony Devaux  <https://orcid.org/0000-0002-8862-4218>

Robin Genuer  <https://orcid.org/0000-0002-0981-3943>

## Supplemental material

Supplemental material including the simulation description and additional tables and figures for the simulation and application is available online. Supplemental materials for this article are available online.

## References

1. Proust-Lima C and Taylor JMG. Development and validation of a dynamic prognostic tool for prostate cancer recurrence using repeated measures of posttreatment PSA: a joint modeling approach. *Biostatistics* 2009; **10**: 535–549.
2. Fournier MC, Foucher Y, Blanche P et al. Dynamic predictions of long-term kidney graft failure: an information tool promoting patient-centred care. *Nephrol Dialysis Transp* 2019; **34**: 1961–1969.
3. Paige E, Barrett J, Stevens D et al. Landmark models for optimizing the use of repeated measurements of risk factors in electronic health records to predict future disease risk. *Am J Epidemiol* 2018; **187**: 1530–1538.
4. Rizopoulos D. *Joint Models for Longitudinal and Time-to-Event Data*. New York, NY: Chapman and Hall/CRC, 2012. ISBN 978-1-4398-7287-1. DOI:10.1201/b12208. <https://www.taylorfrancis.com/books/9781439872871>.
5. Van Houwelingen HC. Dynamic prediction by landmarking in event history analysis. *Scand J Stat* 2007; **34**: 70–85.
6. Ye W, Lin X and Taylor JMG. Semiparametric modeling of longitudinal measurements and time-to-event data-A two-stage regression calibration approach. *Biometrics* 2008; **64**: 1238–1246.
7. Ferrer L, Putter H and Proust-Lima C. Individual dynamic predictions using landmarking and joint modelling: validation of estimators and robustness assessment. *Stat Methods Med Res* 2019; **28**: 3649–3666.
8. Devaux A, Genuer R, Peres K et al. Individual dynamic prediction of clinical endpoint from large dimensional longitudinal biomarker history: a landmark approach. *BMC Med Res Methodol* 2022; **22**: 188.
9. Tanner KT, Sharples LD, Daniel RM et al. Dynamic survival prediction combining landmarking with a machine learning ensemble: methodology and empirical comparison. *J R Stat Soc: Ser A (Statistics in Society)* 2021; **184**: 3–30.
10. Hickey GL, Philipson P, Jorgensen A et al. joinerML: a joint model and software package for time-to-event and multivariate longitudinal outcomes. *BMC Med Res Methodol* 2018; **18**: 50.
11. Rizopoulos D. The R package JMbayes for fitting joint models for longitudinal and time-to-event data using MCMC. *J Stat Softw* 2016; **72**. DOI: 10.18637/jss.v072.i07.
12. Hickey GL, Philipson P, Jorgensen A et al. Joint modelling of time-to-event and multivariate longitudinal outcomes: recent developments and issues. *BMC Med Res Methodol* 2016; **16**: 117.
13. Yao F, Müller HG and Wang JL. Functional data analysis for sparse longitudinal data. *J Am Stat Assoc* 2005; **100**: 577–590.
14. Li K and Luo S. Dynamic prediction of Alzheimer’s disease progression using features of multiple longitudinal outcomes and time-to-event data. *Stat Med* 2019; **38**: 4804–4818.
15. Signorelli M, Spitali P, Szigyarto CAK et al. Penalized regression calibration: a method for the prediction of survival outcomes using complex longitudinal and high-dimensional data. *Stat Med* 2021; **40**: 6178–6196.
16. Jiang S, Xie Y and Colditz GA. Functional ensemble survival tree: dynamic prediction of Alzheimer’s disease progression accommodating multiple time-varying covariates. *J R Stat Soc: Ser C (Applied Statistics)* 2021; **70**: 66–79.
17. Lin J, Li K and Luo S. Functional survival forests for multivariate longitudinal outcomes: dynamic prediction of Alzheimer’s disease progression. *Stat Methods Med Res* 2021; **30**: 99–111.
18. Albert PS and Shih JH. On estimating the relationship between longitudinal measurements and time-to-event data using a simple two-stage procedure. *Biometrics* 2010; **66**: 983–987.
19. Ishwaran H, Kogalur UB, Blackstone EH et al. Random survival forests. *Ann Appl Stat* 2008; **2**: 841–860.
20. Ishwaran H, Gerds TA, Kogalur UB et al. Random survival forests for competing risks. *Biostatistics* 2014; **15**: 757–773.
21. Laird NM and Ware JH. Random-effects models for longitudinal data. *Biometrics* 1982; **38**: 963–974.
22. Gray RJ. A class of K-sample tests for comparing the cumulative incidence of a competing risk. *Ann Stat* 1988; **16**: 1141–1154.
23. Andersen PK, Geskus RB, de Witte T et al. Competing risks in epidemiology: possibilities and pitfalls. *Int J Epidemiol* 2012; **41**: 861–870.

24. Blanche P, Proust-Lima C, Loubère L et al. Quantifying and comparing dynamic predictive accuracy of joint models for longitudinal marker and time-to-event in presence of censoring and competing risks: comparing dynamic predictive accuracy of joint models. *Biometrics* 2015; **71**: 102–113.
25. Gerds TA and Schumacher M. Consistent estimation of the expected brier score in general survival models with right-censored event times. *Biometrical J* 2006; **48**: 1029–1040.
26. Gregorutti B, Michel B and Saint-Pierre P. Grouped variable importance with random forests and application to multiple functional data analysis. *Comput Stat Data Anal* 2015; **90**: 15–35.
27. Proust-Lima C, Sène M, Taylor JM et al. Joint latent class models for longitudinal and time-to-event data: a review. *Stat Methods Med Res* 2014; **23**: 74–90.
28. 3C Study Group. Vascular factors and risk of dementia: design of the Three-City study and baseline characteristics of the study population. *Neuroepidemiology* 2003; **22**: 316–325.
29. Proust-Lima C, Philipps V, Dartigues JF et al. Are latent variable models preferable to composite score approaches when assessing risk factors of change? Evaluation of type-I error and statistical power in longitudinal cognitive studies. *Stat Methods Med Res* 2019; **28**: 1942–1957.